Water Harvesting

Tillandsia-Inspired Hygroscopic Photothermal Organogels for Efficient Atmospheric Water Harvesting

Feng Ni, Nianxiang Qiu, Peng Xiao,* Chang Zhang, Yukun Jian, Yun Liang, Weiping Xie, Luke Yan, and Tao Chen*

Abstract: Tillandsia species with degenerated roots have evolved into hygroscopic leaves that absorb moisture from air. This interesting biological adaptability has inspired us to develop an integrated hygroscopic photothermal organogel (POG) to achieve a solar-powered atmospheric water harvesting (AWH). The well-designed hydrophilic co-polymeric skeleton is fabricated to accommodate hygroscopic glycerin medium, which enables the POG self-contained property, mechanically flexibility and synergistic enhancement of moisture sorption. The integration of interpenetrated photothermal component of poly-pyrrole-dopamine (P-Py-DA) can endow the POG an efficient solar-to-thermal property for controllable solar-driven interfacial water releasing. The integrated POG has an equilibrium moisture sorption of 16.01 $kg\,m^{-2}$ at the RH of 90%, and daily water production as high as 2.43 $kg\,m^{-2}\,day^{-1}$ is achieved in actual outdoor experiments.

Introduction

Freshwater scarcity has been increasingly perceived as a challenge worldwide, threatening society development and even human life, and is urgently to be solved.[1] Since earth's atmosphere contains ubiquitous and huge water vapor resources of about 50000 km³ that is rarely exploited, there has been intense interest in harvesting water from air for purified water production.[2] Recently, a technology of combined moisture sorption from air and solar-heated releasing is emerging as a promising solution to produce freshwater.[3] For instance, porous materials based on hydration effect can function as effective atmospheric water harvesters. As one typical example, porous metal-organic framework (MOF) enables active capturing of atmospheric water vapor at relatively low humidity and then releases water powered by sunlight.[4] Owing to their premature sorption saturation, these MOF sorbents performed a relatively lower hygroscopic capacity under high RHs (> 50% RH) and only worked in a narrow RH range.[3b,4d,5] Also, the highly hydrophilic hydrogel-based sorbents (mainly aerogel or xerogel) can experience a hygroscopic process via hydrogen bonding and further contain abundant water molecules inside the three-dimensional (3D) cross-linked network in the form of swelling.[2a,6] Yet, due to the relatively low diffusion rate inside the dried network, the hydrogel-based sorbents may suffer from unsustainable sorption capability once water molecules completely cover their surface.[7] On the other hand, the porous structure of these hydrogel-based sorbents can experience a potential risk of collapse, either in the preparation procedures or the water sorption-desorption cycles, resulting in a performance decline in moisture sorption. Moreover, the alternative integration of solid sorbents into the abovementioned porous materials can prominently enhance the sorption capacity via the synergistic mechanism of physical and chemical sorption.[6b,7,8] However, salts agglomeration and leakage during hydration/dehydration cycles still remain a challenge for practical AWH application.

As a promising alternative for atmospheric water capturing, liquid sorbents can achieve high sorption capacity mediated by an osmotic-effect-enabled rapid water diffusion in concentrated sorbents.[9] Superior to the hydrophilic solid sorbent, the liquid system demonstrates promoted capability of reactivating the sorption binding sites for high-capacity moisture sorption.[3a] Attributed to the lack of contained network, yet the liquid sorption system with flowable characteristics remains some problems, such as unfavorable sorbents leakage, poor portability and non-integrated structure for the sorption-desorption process. Hence, it is highly desirable for a self-contained, highly absorbable and integrated hygroscopic photothermal material system for atmospheric water harvesting in a low-grade energy consumption.

[*] F. Ni, Dr. P. Xiao, C. Zhang, Y. Jian, Y. Liang, Prof. T. Chen
Key Laboratory of Marine Materials and Related Technologies,
Zhejiang Key Laboratory of Marine Materials and Protective Technologies, Ningbo Institute of Materials Technology and Engineering,
Chinese Academy of Sciences
Ningbo 315201 (China)
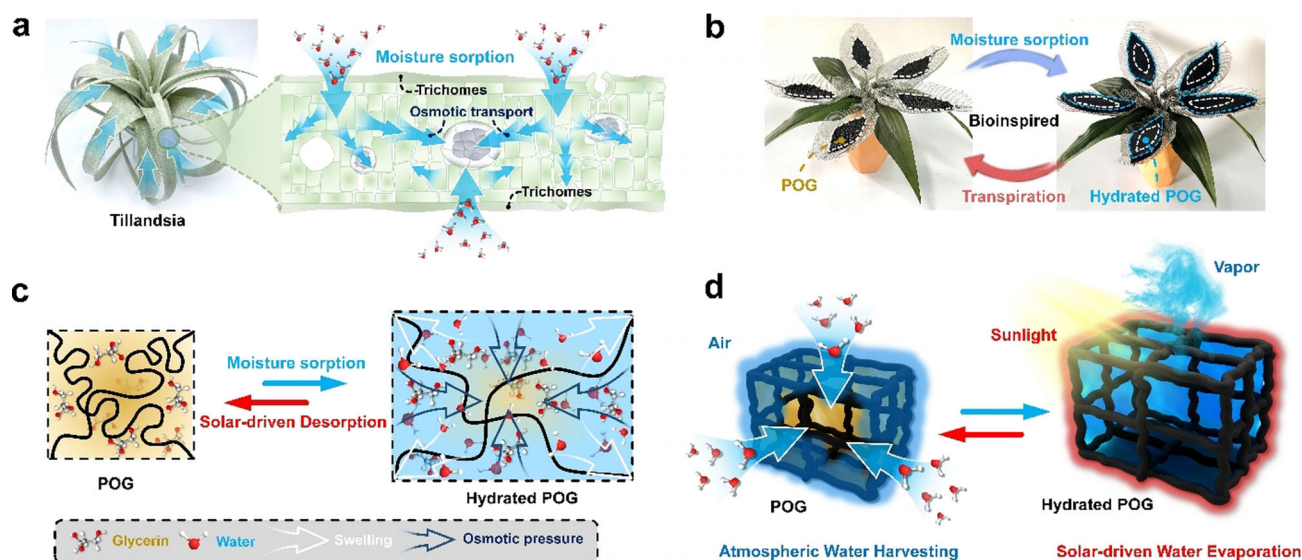E-mail: xiaopeng@nimte.ac.cn
        tao.chen@nimte.ac.cn

F. Ni, Dr. P. Xiao, Y. Jian, Y. Liang, Prof. T. Chen
School of Chemical Sciences
University of Chinese Academy of Sciences
Beijing 100049 (China)

Dr. N. Qiu
Engineering Laboratory of Advanced Energy Materials
Ningbo Institute of Material Technology and Engineering
Chinese Academy of Sciences, Ningbo (China)

W. Xie
Analytical Center, Ningbo Institute of Material Technology and
Engineering, Chinese Academy of Sciences
Ningbo (China)

Prof. L. Yan
Polymer Materials & Engineering Department, School of Materials
Science & Engineering, Chang'an University
Xi'an 710064 (P. R. China)

Supporting information and the ORCID identification number(s) for the author(s) of this article can be found under:
https://doi.org/10.1002/anie.202007885.

Wiley Online Library

These are not the final page numbers!

© 2020 Wiley-VCH GmbH

Angew. Chem. Int. Ed. **2020**, 59, 2 – 12

Scheme 1. The concept of Tillandsia-inspired hygroscopic POG for Atmospheric water harvesting. a) The moisture sorption of Tillandsia from the air for its life activities. b) Illustration of Tillandsia-inspired hygroscopic POG that can imitate the moisture-sorption and transpiration behaviors of the Tillandsia. c) The high capacity of moisture sorption of the integrated POG. The water molecules are captured on the surface of the POG, then transported into its interior via osmotic pressure, and stored inside POG through swelling. d) The solar-driven atmospheric water harvesting based on the achieved POG.

Natural plants have provided instructive examples of biological moisture-absorbing system. As an interesting representative of epiphytic plants, Tillandsia species have adaptively evolved hygroscopic leaves to replace the degenerated roots, which are capable of trapping moisture from atmosphere.[10] The liquefied water aggregated on leaf surface can be further guided by a directed transportation from outermost tissues to interior network via active osmotic effect (Scheme 1a). The well-established tissue systems can effectively hold the absorbed water and regulate the leaf transpiration for sustainable growing requirements. Inspired by hygroscopic Tillandsia, we propose here an integrated hygroscopic photothermal organogel (POG) to capture atmospheric moisture and further empower in situ interfacial solar release. The integrated hygroscopic material system arises from the programmable combination of hydrophilic copolymeric network of sodium polymethacrylate/polyacrylamide (P(SMa-co-AAm)), hygroscopic glycerin medium. Note that the synergistic hygroscopic effect can be effectively regulated by adjusting monomer ratios of polymer network and solvent displacement factors. Further integration of photothermal poly-pyrrole-dopamine (P-Py-Da) can endow the hygroscopic system efficient solar-to-thermal property for controllable water releasing. Remarkably, the resulted POG can imitate the foliar moisture-sorption and transpiration behavior of the Tillandsia (Scheme 1b). The combination of hydrophilic co-polymeric network and hygroscopic glycerin medium allows the POG to absorb moisture from the air, transport it to the interior via osmotic pressure and store it in form of swelling of polymeric chains for a high-capacity moisture sorption (Scheme 1c). As a result, such a POG can be applied to experience a cycle of atmospheric water harvesting and solar-driven water evaporation for freshwater production (Scheme 1d).

Results and Discussion

Preparation and Characterization of the POG

The key to the construction of the hygroscopic POG lies in the design of a precursor photothermal hydrogel (PHG). The detailed synthetic procedures are illustrated in Figure 1a. To enable polymeric gel an ideal photothermal property, an aqueous dispersion of P-Py-DA was first fabricated, as shown in the Supporting Information, Figure S1. Owing to the alternative introduction of dopamine in the polymerization of pyrrole, the dispersion of the resulted nanoscale P-Py-DA in the water could maintain a more stable state than that of pure PPy, benefiting for the subsequent synthesis of hydrogel. Next, a cross-linked photothermal P(SMA-co-AAm) hydrogel was formed from in situ copolymerization of acrylamide (AAm), sodium methacrylate (SMa), methylene-bis-acrylamide (MBAA) crosslinker and aqueous dispersions of P-Py-DA using ammonium persulfate (APS) as thermal initiator, as our reported previously.[11] The sodium polymethacrylate (PSMa) with plentiful oxygen-containing functional groups was chosen due to its intrinsic characteristics of hydrophilicity and swelling. Further copolymerization of polyacrylamide (PAAm) was rationally designed to adjust the storage capacity of glycerin. After that, the solvent displacement was applied to replace the water in the above hydrogel by hygroscopic liquid medium.[12] Herein, owing to its characteristics of strong hygroscopicity, harmlessness, high evaporation temperature and extremely low cost, the glycerin was selected as a representative hygroscopic organic liquid for constructing POG. Accordingly, the as-fabricated PHG was directly immersed in the excess pure glycerin for solvent displacement (Figure 1b). During the above period, water molecules in the PHG exchanged with the external glycerin molecules, until be

These are not the final page numbers!
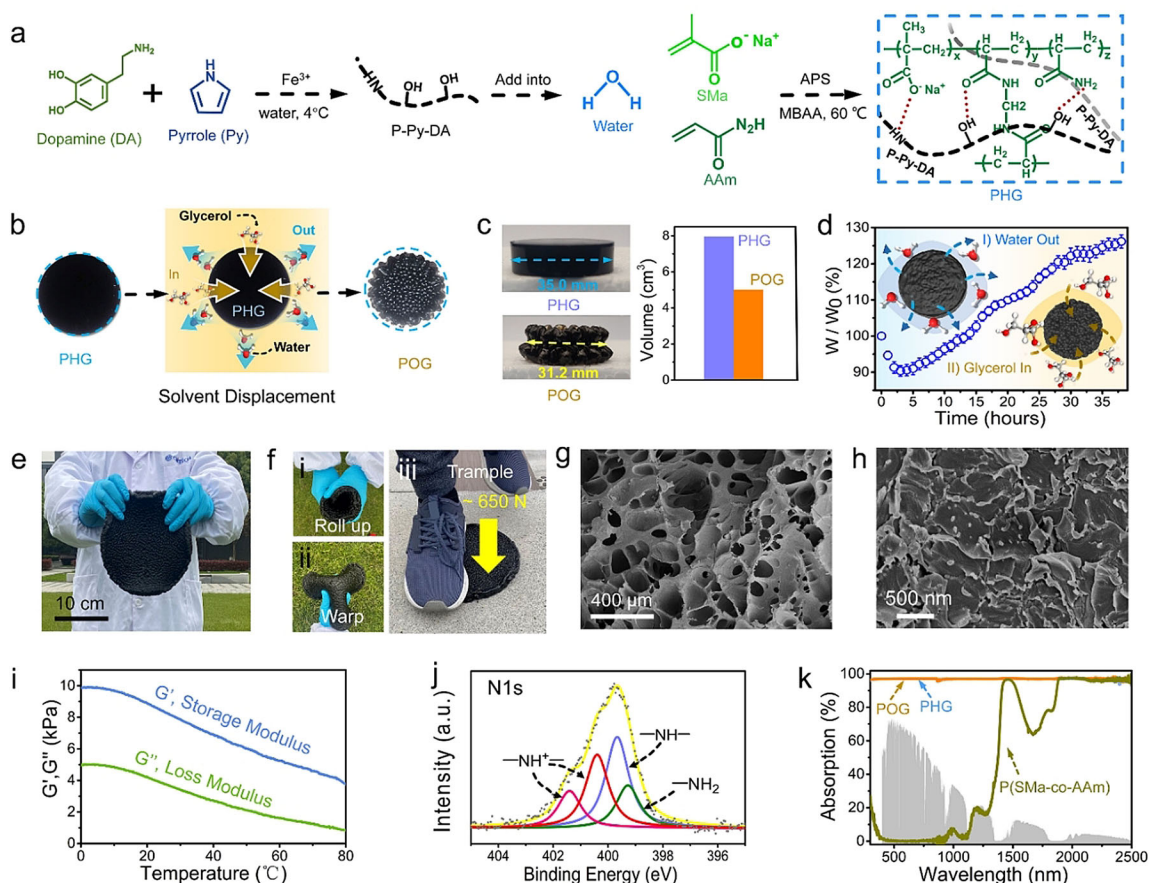
Figure 1. The preparations and characterizations of the POG. a) The synthetic procedures and the molecular structures of the PHG. b) Top-view photographs of the achieved PHG and POG. c) Side-view photographs and the volumes of PHG and POG, respectively. d) The mass change of the sample during the solvent exchange. e) Physical picture of a large-scale piece of the POG. f) The as-prepared POG is highly flexible, which can endure a large-degree roll up, warp and even trample of a 65-kg man. g),h) SEM images of the polymeric skeleton of the POG. i) Rheological properties of the POG, the storage modulus G′ is always greater than the loss modulus G″ at all measured temperatures, revealing a stable crosslinked structure in a high temperature. j) High resolution XPS spectrum for N 1s of the polymer networks of the POG. k) The solar absorption spectra of the POG, PHG and P(SMa-co-AAm), respectively, demonstrate POG have nearly identical solar absorption with PHG, which is much higher than that of P(SMa-co-AAm) hydrogel.

completely replaced by glycerin, thereby obtaining the POG. Photographs of the achieved PHG and POG were shown in Figure 1b, demonstrating significant changes on the surface structure and dimensions after solvent displacement. Compared with the initial PHG, a pleated structure appeared on the surface of the resulted POG, which was probably caused by asymmetric exchange of glycerin and water. Moreover, the diameter of the achieved POG shortened to 31.2 mm from 35 mm of the original PHG, and its volume also decreased from 7.96 to 5.02 cm^3 (Figure 1c). As shown in Figure 1d, the mass change of polymeric gel during the whole solvent displacement was monitored. The exchange of water with glycerin was a bidirectional procedure, including extraction of water molecules and importation of glycerin molecules. During first 4 hours, the inner water molecules in PHG could rapidly discharge to the external environment driven by osmotic pressure, which was faster than speed of glycerin input, thus the mass of the polymeric gel declined. Then, since the continuous swelling of the gel in glycerin, the weight of gel started increasing, and finally reached to 127% of its initial weight after 39 hours of solvent displacement to obtain the

POG. As a result, this facile and general preparing strategy easily allows the formation of a large-area POG with the diameter of about 17 cm (Figure 1e). In addition, the resulted POG exhibits a more excellent mechanical flexibility and strength than the initial PHG, and can withstand a large-degree roll up, warp and even trample of a 65-kg man (Figure 1f; Supporting Information, Figure S2).

The microstructures of the polymeric skeleton of the POG were observed by scanning electron microscope (SEM), as demonstrated in the Figure 1g,h. We can observe the abundant interconnected pores with the width varying from a few microns to tens of microns in the POG, which can serve as spaces for storing and hold hygroscopic liquid sorbent (Figure 1g). As displayed in the Figure 1h, compared with the smooth surface of the network of P(SMa-co-AAm) hydrogel (Supporting Information, Figure S3), the skeleton of the POG (P-Py-DA/P(SMa-co-AAm)) seemed much rougher due to P-Py-DA embedded on the its surface.

From results of rheological characterization, the value of storage modulus (G′) and the loss modulus (G″) of the P-Py-DA/P(SMa-co-AAm) are both lower than those of P(SMa-co-

AAm), which reveals that two polymer chains, P-Py-DA and P(SMa-co-AAm), are inserted into each other to form an interpenetrating polymeric skeleton in the POG (Supporting Information, Figure S4).[13] Meanwhile, the value of G′ is higher than that of the G″ in the frequency range of 0.1–100 Hz, indicating the skeleton of the POG was a crosslinked gel network (Supporting Information, Figure S5). Importantly, the POG can maintain this crosslinked structure at measured temperature up to 80 °C, which ensures its operation stability in the subsequent photothermal evaporation (Figure 1 i).

To further clarify chemical composition of the polymeric skeleton of the POG, Fourier transform infrared spectroscopy (FTIR) was conducted, as displayed in the Supporting Information, Figure S6. Owing to introduction of P-Py-DA in the synthesis of polymer network, new peaks at 996 cm^{-1} and 1617 cm^{-1} appear in the spectra of P-Py-Da/P(SMa-co-AAm), attributing to the C−H and C=C out-of-plane deformation vibration, respectively.[14] In addition, abundant hydroxyl groups (at 3423 cm^{-1}) enable the polymeric skeleton of the POG a high affinity to water molecules, which is conducive to its moisture sorption.[14a, 15] In the XPS characterization of polymeric network in the POG, the amino-like (-NH$_2$) and amine-like (-NH-) structures are located at the binding energy of 399.2 eV and 399.7 eV, respectively, while the peaks at 400.4 eV and 401.41 eV can be attributed to charged nitrogen species (-NH$^+$-) (Figure 1 i).[16] These N peaks of the skeleton in the POG slightly upshifted from those of the P(SMa-co-AAm), resulting from hydrogen bonds between P-Py-Da and P(SMa-co-AAm) chains (Supporting Information, Figure S7). The ability of light absorption of materials is a key factor for achieving a high-efficient solar-driven water desorption.[17] As shown in the Figure 1 j, the resulted PHG and POG can reach almost identical light absorption of up to 97 % in the wavelength from 400 to 2500 nm, while P(SMa-co-AAm) hydrogel demonstrates an insufficient light absorption of 50 %.

Atmospheric Moisture Sorption of the POG

The hypothesis of possible POG moisture sorption process is presented and schematically illustrated in Figure S8. Since the strong polarity of characteristic groups on its surface, such as hydroxyl and carboxyl groups, the POG performed high hygroscopicity, and thus could easily capture the water molecules from the air via hydrogen bonds interactions. Afterwards, the absorbed water molecules could further diffuse into the interior of the POG guided by the osmotic pressure of inner glycerin medium, which could quickly reactivate sorption bonding sites on the surface. Moreover, these water molecules would replace positions of glycerin molecules on the polymer skeleton through the breaking old hydrogen bond and forming new one, which could simultaneously release the initial bonded glycerin molecules for new sorption and transportation of water. As a result, these relevant features enable the achieved POG the capacity of sustainable and high-capacity moisture sorption. To indirectly observe the moisture sorption process, In Situ

Raman mapping is characterized to track the sorption path of water molecules on POG surface. Since there are both O−H bonds existed in water and glycerin (Supporting Information, Figure S9), Raman band ratio that is defined as the intensity ratio of I$_1$ (C−H bonds of stretching vibration area within 2800–3000 cm^{-1}) and I$_2$ (O−H bonds of stretching vibration area within 3050–3600 cm^{-1}) is presented to achieve a real-time signal monitoring. The Raman spectrum of the synthesized POG surface after solvent displacement was demonstrated in Figure 2 a. With the increasing of moisture sorption time, the ratio of integrated intensity of I$_2$ with I$_1$ is gradually elevated, indicating that the content of water molecules adsorbed on the POG surface experiences an increasing trend (Supporting Information, Figure S10). To visually observe this dynamic moisture sorption process, a two-dimensional (2D) mapping (20 × 20 μm) was recorded. A prominent color change, referring to I$_2$/I$_1$, can be observed on Raman mappings as the moisture sorption processes, which suggests the POG surface has a capacity of capturing water molecules from the air (Figure 2 b). In comparison with initial state (Supporting Information, Figure S11), the 60-min POG has undergone a huge change on the color of Raman mapping, implying that its surface has been completely occupied by water molecules. Moreover, the vertical water molecules diffusion was also captured in the cross-sectional Raman mapping. As displayed in Figure 2 c, an obvious color gradient exists in the POG after 180 min moisture sorption, which reveals that water molecules can be effectively transported to the interior of the proposed organogel materials system. The abovementioned results illustrate that water molecules in air can be effectively captured by the surface of POG and subsequently transported to the inner.

To further elevate the capacity of moisture sorption of POG, the composition of polymeric skeleton is systematically studied. As a stretchable container for glycerin sorbent, the composition of polymeric skeleton not only determined the amount of glycerin carried, but possibly played a synergistic role in the water sorption due to its inherent hydrophilic feature. In our system, the glycerin content in the POG could be modulated by changing the weight ratio of SMa and AAm monomer in the synthesis of its polymer networks. As demonstrated in the Supporting Information, Figure S12, the weight of glycerin in POG with SMa to AAm ratio of 7:1, 3:1, 5:3, 1:1, 3:5 and 0:1 could reach 4.2, 4.8, 5.4, 5.5, 4.9, and 2.3 times than that of its polymeric skeleton, respectively. The corresponding hygroscopic performances were illustrated in the Figure 2 d, which demonstrated that the glycerin played the major role during the moisture sorption in the POG system. Owing to the relatively strong polarity of the polymer chains, the absorbed water molecules are considered to be dynamically captured and replace the binding sites of glycerin molecules on hydrophilic polymer backbone. Then, the glycerin molecules could be efficiently released to absorb or transport new water molecules for improving the capability of the moisture sorption. Therefore, the hydrophilic polymer network may also have a synergistic effect on the moisture sorption capacity of the POG. In order to understand how the hydrophilic polymeric skeleton plays the synergistic effect in moisture sorption process, a control experiment of POG and
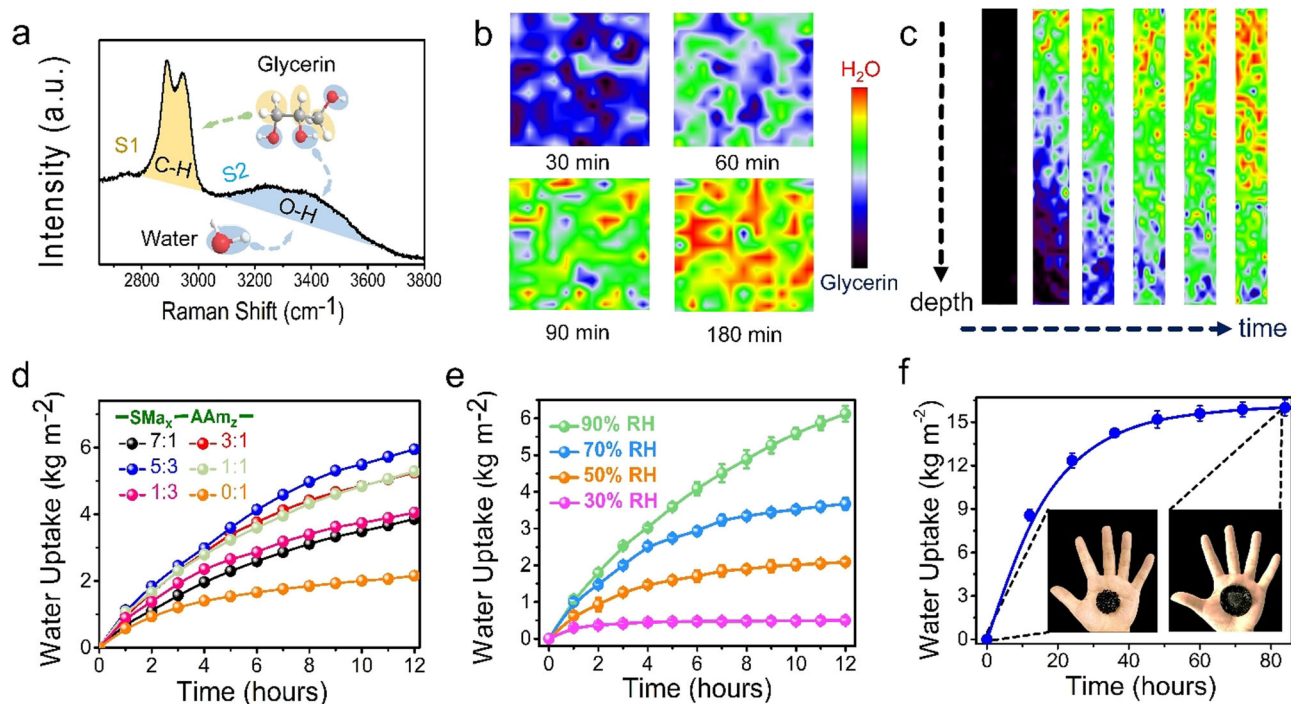
Figure 2. Moisture sorption from the air with the POG. a) Raman spectrum of the POG surface, in which I_1 and I_2 refer to the integrated intensities of characteristic regions of C—H and O—H bonds, respectively. b) In situ Raman mappings after absorbing moisture show the POG surface have been occupied by water molecules after 180 min of water sorption. c) Raman mapping of the region from the surface to the interior of the POG along the direction of water transport after 0, 10, 30, 60, 120, 180 min of moisture sorption, respectively. The depth and width of the regions was 20 μm and 500 μm, respectively. d) The moisture sorption of POGs with different polymeric networks reveals POG has the best moisture sorption performance when the monomer ratio of SMA and AAm is 5:3. e) The performance of moisture sorption of the optimized POG under varied RH from 30% to 90%. f) The long-term moisture sorption of the POG under the 90% RH, the insert images are the initial POG and the hydrated POG, respectively, which shows the hydrated POG has an obvious swelling.

pure glycerin samples with the same hygroscopic area and thickness were conducted in the Supporting Information, Figure S13. The results clearly illustrated that POG presented a stronger hygroscopic performance than that of glycerin liquid. Accordingly, the above results revealed that hygroscopic glycerin medium played a major role in absorbing moisture. The rational combination of hydrophilic polymer chains could play a synergistic role in the moisture sorption process. As a result, the largest amounts of moisture sorption of the POG within 12 h was 5.95 kg m^{-2} when the ratio of SMa to AAm was 5:3 at 90% RH and 25°C (Figure 2d). Furthermore, the external factor of relative humidity (RH) can also significantly affect the moisture sorption performance. As shown in Figure 2e, the moisture sorption performance of the optimized POG was further examined quantitatively at 25°C under different RHs. The optimized POG demonstrated the water sorption capacity of 6.12, 3.67, 2.09, and 0.50 kg m^{-2} at 90%, 70%, 50%, and 30%, respectively, which were competitive to those from recently published literature, as shown in the Supporting Information, Figure S14.[9a] The water sorption isotherms of POG were also displayed in the Supporting Information, Figure S15. More importantly, benefiting from the integration of polymeric skeleton and glycerin sorbent, such an integrated POG showed a superhigh equilibrium moisture sorption of 16.01 kg m^{-2} (ca. 1.54 g g^{-1}) under 90% RH for 84 hours.

Moreover, the hydrated POG could hold and keep the absorbed water in its interior in the form of swelling without leakage. As a result, the POG demonstrated a significant volume-expansion phenomenon after experiencing above long-term water vapor sorption, whose volume increase up to 34.5 from 5.02 cm^3 (Figure 2 f).

Mechanism for Continuous and High-Capacity Moisture Sorption of the POG

In our former hypothesis, the absorbed water molecules could be captured by hydrophilic functional groups and further transported from the surface to inner POG via the osmotic pressure of glycerin medium to synergistically enhance the hygroscopic performance. The coherent water capture and diffusion process is considered to dominate the continuous and high-capacity performance of moisture sorption. To further verify the potential mechanism, molecular dynamics (MD) simulation was conducted to elaborate the sorption, transport behavior and recombination process of water molecules (Supporting Information, Figures S16–S18).

As shown in the Figure 3a, a computing model capable of reproducing the essentials of sorption and transportation process of water molecules in the POG was established. The MD results clearly revealed that water molecules were
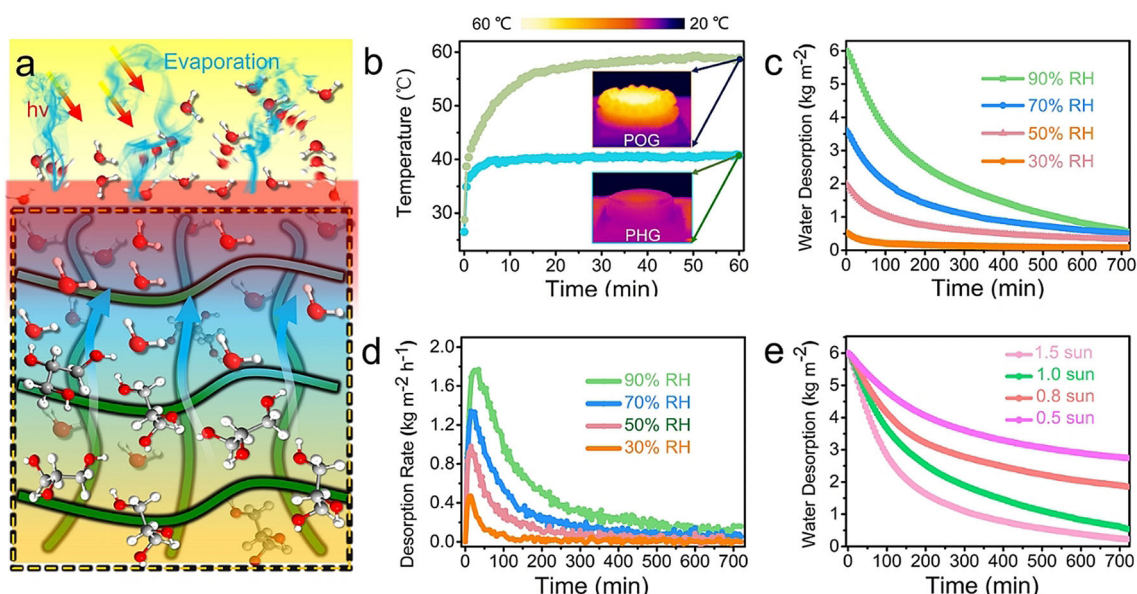
These are not the final page numbers!
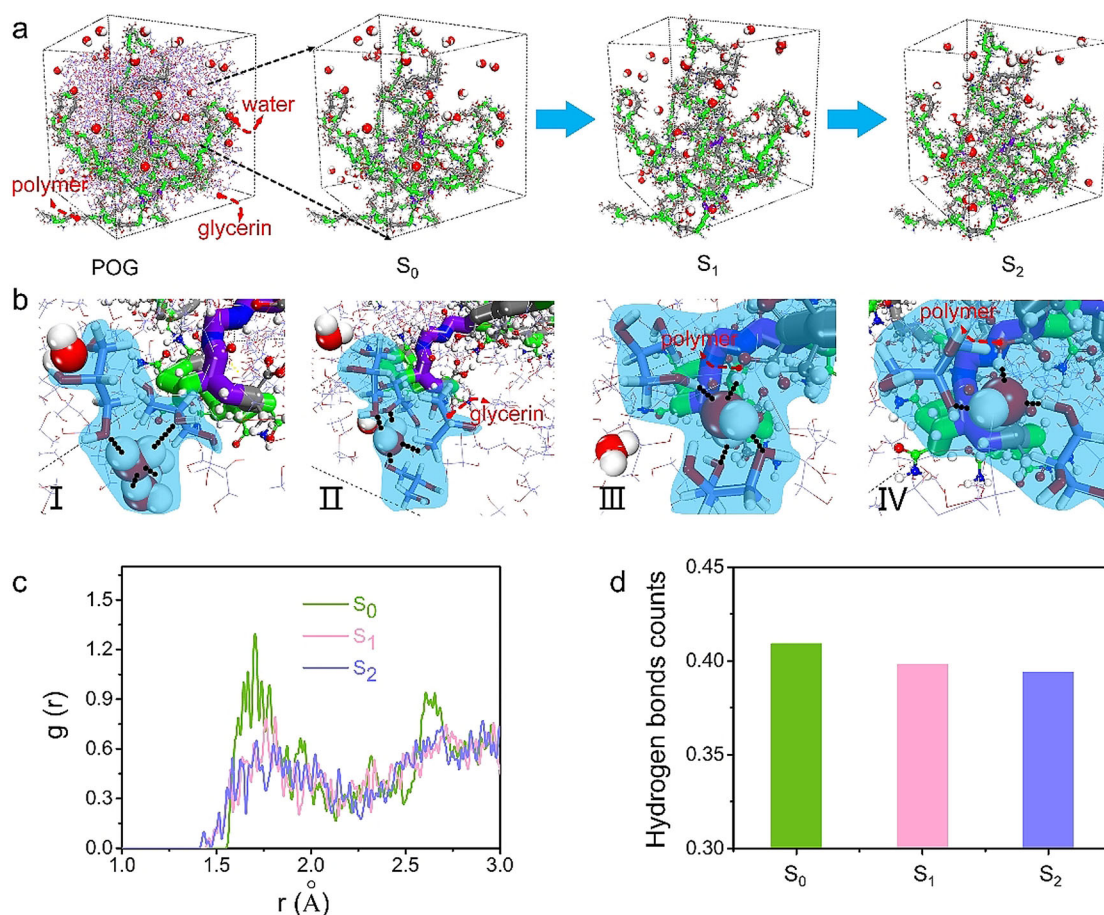
Figure 3. Molecular dynamics (MD) simulation results of the sorption and transportation behaviors of water molecules of the POG. a) The computing model of the hydrated POG demonstrates absorbed water molecules can be captured, then transported to the interior due to the osmotic effect of glycerin molecules, and eventually bonded with hydrophilic polymer skeleton through hydrogen bonds. The S_0, S_1 and S_2 refer to the time of 0 s, 3 ns, and 6 ns for water transportation, respectively. b) Snapshots of a specific water molecule transported from the outside to the internal polymeric chains. The black dotted lines represent the hydrogen bonds between the specific water molecule and surrounding molecules. c) The pair-correlation function of pairs between -OH of glycerin and -NH_2, -C(O)OH of polymer chains at the S_0, S_1 and S_2, respectively. d) Normalized numbers of corresponding hydrogen bonds in the (c).

transported into the interior from the exterior of the POG due to osmotic effect, which could reactivate the absorbing sites on the POG surface for a rapid moisture sorption. Moreover, the transportation of specific water molecule in the POG was tracked to understand the interactions between water molecules and surrounding molecules (Figure 3b). 1) It can be observed that a selected water molecule was contained in a three-water-molecules cluster and bonded two glycerin molecules at the initial time; 2) then the water molecule was bonded with four glycerin molecules and transported driven by the osmotic pressure of glycerin; 3) eventually, the selected water molecule replaced the position of glycerin molecule and linked on the polymer chain though hydrogen bonds; 4) after a period of moisture sorption, this water molecule still bond with polymeric skeleton. In addition, the pair-correlation function ($g(r)$) of pairs between -OH of glycerin and -NH_2, -C(O)OH of polymer chains at the S_0, S_1 and S_2, respectively, is computed to predict the interactions between polymer chains and glycerin, which is an effective way to understand the process of replacement of glycerin molecules bonded on the polymeric skeleton by absorbed water molecules (Fig-

ure 3c). The r value refers the distance between two target molecules (or atoms), and the $g(r)$ value represents the probability of a molecule (or atom) pair within a specific r value.

As a result, the peaks around 2.0 Å, referring to the pairs between target molecules, gradually decreased as the moisture sorption proceeds, which indicated the amount of interactions between glycerin and polymer chains was declining. Additionally, the number of corresponding hydrogen bonds between glycerin and polymer chains during above period was calculated in the Figure 3d, which also showed a downward trend. Therefore, the water molecules transported to the interior could be linked on the hydrophilic polymer chains through replacing initial bonded glycerin molecules, allowing these glycerin molecules to capture of new water molecules. Therefore, combined with the aforementioned theoretical simulation, the potential moisture sorption mechanism could be proposed. When captured on the POG surface, water molecules were transported into the interior of the POG under the action of osmotic pressure, which could quickly reactivate absorbing sites on the POG

Angew. Chem. Int. Ed. 2020, 59, 2–12

© 2020 Wiley-VCH GmbH

www.angewandte.org

These are not the final page numbers!↗↗

Figure 4. The interfacial water desorption of the hydrated POG under solar illumination. a) The water desorption of hydrated POG by an interfacial solar-driven evaporation. b) The temperature changes of POG and PHG over time show POG can reach to a higher temperature than that of PHG under 1.0-sun illumination. c) Water desorption and d) Desorption rate of POG hydrated in different humidity over time under 1.0-sun illumination. e) Water desorption of POG hydrated in 90% RH for 12 hours over time under different intensities of solar illuminations.

surface for a continuous and high-capacity moisture sorption. Moreover, the hydrophilic polymer chains in the POG can catch the adjacent absorbed water molecules via the new formed hydrogen bonds and simultaneously release the bonded glycerin for new moisture sorption, thus can play a synergistic role in the moisture sorption. Notably, we developed a new material system of organogel for AWH, which may provide a reference for the design of the subsequent hygroscopic materials. The selection of the polymeric skeleton and hygroscopic medium of the organogel is highly designable. Also, the moisture-sorption performances of the POG over the entire RH range have the potential to be further improved by their rational design, such as replacing more hygroscopic organic solvents, doping inorganic salts, etc.

The Interfacial Solar-Driven Water Desorption of the Hydrated POG

Although strong interactions between the POG and water molecules can realize efficient moisture sorption of the POG from the air, it will also hinder its water desorption. As illustrated in the Figure 4a, the POG can generate a large amount of thermal energy because of its superior photo-to-thermal conversion and localize it on the surface, thus providing sufficient energy to break interactions between water and the POG for efficient water desorption.[18] Compared with the PHG, the resulted POG could reach to a higher temperature under the same solar irradiation attributing to smaller specific heat capacity of glycerin (Figure 4b). The water desorption isobar of the hydrated POG at 30% R.H. was shown in the Supporting Information, Figure S19. In addition, the hydrated POGs absorbing moisture for 12 hours at different RHs were examined the

desorption performance under solar illumination of 1.0 kw m^{-2}. It was observed that corresponding surface temperatures of the POG rapidly increased at first 100 min, and subsequently rose slowly as the water content decreased (Supporting Information, Figure S20). As a result, hydrated samples could experience a huge water desorption after solar illumination of 12 h, in which the POG treated with 90% RH, 70% RH, 50% RH, 30% RH could achieve the water release of 5.52, 3.11, 1.68, 0.43 kg m^{-2}, respectively (Figure 4c). As shown in the Figure 4d, water desorption rate of the hydrated POG initially increased and then decreased, demonstrating a parabola-like trend. It is noteworthy that the maximum rate of water desorption for the hydrated POG was up to 1.77 kg m^{-2} h^{-1}.

Moreover, we selected the hydrated POG treated with 90% RH for 12 h to further evaluate its water desorption performance under different solar intensities varying from 0.5 to 1.5 sun. The equilibrium temperatures of the selected POG surface could reach to 74.4, 59.4, 52.1 and 44.7 °C, respectively, and its related maximum water desorption rate was 0.77, 1.44, 1.77, 2.41 kg m^{-2} h^{-1} under 0.5, 0.8, 1.0 and 1.5 sun, respectively (Supporting Information, Figures S21 and S22). As a consequence, the amounts of water desorption under 0.5, 0.8, 1.0 and 1.5 sun were 5.78, 5.52, 4.15 and 3.26 kg m^{-2}, respectively (Figure 4e). Note that its inner glycerin would not be squeezed out in the dehydration process, which indicated that POG had a stable structure even after undergoing significant volume shrinkage (Supporting Information, Figure S23).

www.angewandte.org

© 2020 Wiley-VCH GmbH

Angew. Chem. Int. Ed. 2020, 59, 2 – 12

These are not the final page numbers!

Outdoor Experiments Based on the POG to Harvest Purified Water from the Air

To validate the feasibility of the proposed POG for solar-driven atmospheric water harvesting in natural environment, the outdoor experiments were performed on the roof of Materials Building of NIMTE, CAS. Figure 5a showed a schematic photo of POG absorbing moisture from air at night, which was put on the electronic balance to realize the record of mass change. As shown in the Figure 5b, the moisture sorption experiment was carried out from 19:00 to 7:00 the next day, where the ambient temperature and RH
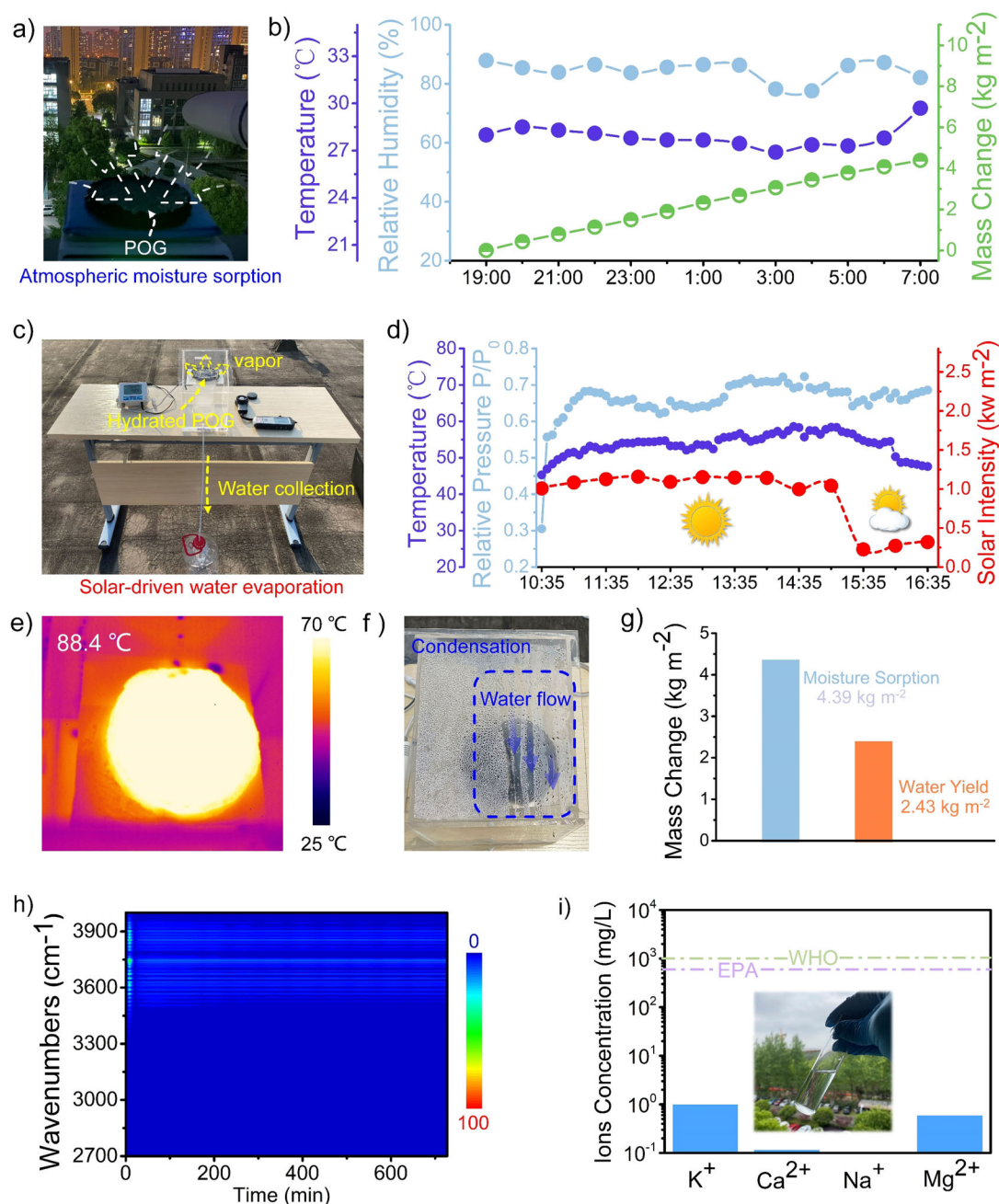
Figure 5. The outdoor experiments based on the POG to harvest purified water from the air. a) The POG during atmospheric moisture sorption at night. b) Profiles of environmental temperature, relative humidity, and mass changes in the outdoor hygroscopic experiment over time. c) Photo of solar-driven water evaporation at daytime in the natural environment. d) The variety of water vapor pressure and temperature inside the device and external solar intensity changes during the practical solar-driven water evaporation. e) The IR photo of the POG under the solar irradiation shows its temperature could reach to 88.4 °C when water evaporated. f) The generated vapor could be naturally condensed into the water droplets, then aggregated into the water flows and slipped down along the device wall. g) The mass change of the POG in the actual AWH, demonstrating the water uptake of 4.36 kg m^{-2} and a water yield of 2.43 kg m^{-2} in the illustrated environmental conditions. h) Time-resolved IR spectroscopy of gas evaporated by hydrated POG and the result shows only water can be released, and glycerin cannot be evaporated even under a high temperature of 100 °C. The color bar refers to normalized intensities of infrared peaks of the gas evaporated from the POG during heating. i) Measured ions concentration in the collected purified water.

were traced per hours. In the night, the average temperature and RH were about 27.89 °C and 84.39 %, respectively, yielding a water uptake of about 4.39 kg m^{-2} for the POG. During the daytime, the resulted hydrated POG was put in a home-made evaporation device for freshwater collection under natural solar illumination (Figure 5 c). The variety of water vapor pressure and temperature inside the device and the external solar intensity changes in the entire solar-driven water evaporation were illustrated in the Figure 5 d. Driven by the thermal energy, the temperature of the POG gradually increased to 88.7 °C (Figures 5 e), and the water absorbed was re-evaporated from the hydrated POG. The hot water vapor could be naturally condensed on the device wall, where purified water generation was visibly manifested via the appearance of water droplets, agglomeration and streaming (Figures 5 f). As a result, we could achieve the freshwater output of 2.43 kg m^{-2} day^{-1} based the resulted POG under solar illumination of an average intensity of 0.90 kw m^{-2}, which was competitive with pervious works based liquid sorbent.[9a] In order to verify the stability of the inner glycerin when using POG under solar illumination, the evaporated gas was characterized to distinguish if it contained glycerin molecules via Time-resolved IR spectroscopy (Figure 5 h). From the results, the characteristic peaks of evaporated gas were concentrated in the region of 3300–4000 cm^{-1}, attributing to O−H bonds, and characteristic peaks of C−H bonds were difficult to find its footprint in the region of 2500–3000 cm^{-1}, indicating there was no glycerin molecules in the evaporated gas. In addition, the measured ions concentration in the collected freshwater were analyzed and the results showed that four primary ions (K$^+$, Ca^{2+}, Na$^+$, Mg^{2+}) were fully compliant with drinking water standards of WHO and EPA (Figure 5 g).

Conclusion

A Tillandsia-inspired hygroscopic POG is developed for efficient solar-driven atmospheric water harvesting. The well-designed hydrophilic co-polymeric network with interpenetrated photothermic component is fabricated to accommodate hygroscopic glycerin medium, enabling the POG self-sustained, highly water-adsorptive, mechanically flexible and photothermal properties. The synergetic effect of hydrophilic polymer network and hygroscopic liquid sorbent of POG can provide an osmotic-effect-enabled rapid water diffusion, which can reactivate sorption binding site for a high-efficient and continuous moisture sorption with the capacity of an equilibrium moisture sorption of 16.01 kg m^{-2} at RH of 90 %. The integrated photothermic P-Py-Da can further release the absorbed water molecules, enabling the purified water production of 2.43 kg m^{-2} day^{-1} in a practical outdoor experiment. Therefore, the bio-inspired hygroscopic POG provides a new pathway for efficient solar-driven atmospheric water harvesting.

[1] a) M. M. Mekonnen, Y. A. Hoekstra, *Sci. Adv.* **2016**, *2*, e1500323; b) Q. Schiermeier, *Nature* **2014**, *505*, 10.

[2] a) F. Zhao, X. Y. Zhou, Y. Liu, Y. Shi, Y. F. Dai, G. Yu, *Adv. Mater.* **2019**, *31*, 1806446; b) Y. D. Tu, R. Z. Wang, Y. N. Zhang, J. Y. Wang, *Joule* **2018**, *2*, 1452; c) J. H. Humphrey, J. Brown, O. Cumming, B. Evans, G. Howard, R. N. Kulabako, J. Lamontagne, A. J. Pickering, E. N. Wang, *Lancet Planet. Health* **2020**, *4*, e91.

[3] a) X. Zhou, H. Lu, F. Zhao, G. Yu, *ACS Mater. Lett.* **2020**, *2*, 671; b) A. LaPotin, H. Kim, S. R. Rao, E. N. Wang, *Acc. Chem. Res.* **2019**, *52*, 1588.

[4] a) S. Y. H. Kim, S. Rao, S. Narayanan, E. A. Kapustin, H. Furukawa, A. S. Umans, O. M. Yaghi, E. N. Wang, *Science* **2017**, *356*, 430; b) H. Kim, S. R. Rao, E. A. Kapustin, L. Zhao, S. Yang, O. M. Yaghi, E. N. Wang, *Nat. Commun.* **2018**, *9*, 1191; c) A. J. Rieth, A. M. Wright, G. Skorupskii, J. L. Mancuso, C. H. Hendon, M. Dinca, *J. Am. Chem. Soc.* **2019**, *141*, 13858; d) N. Hanikel, M. S. Prevot, O. M. Yaghi, *Nat. Nanotechnol.* **2020**, *15*, 348; e) M. J. K. F. Fathieh, E. A. Kapustin, P. J. Waller, J. J. Yang, O. M. Yaghi, *Sci. Adv.* **2018**, *4*, eaat3198; f) D. Ma, P. Li, X. Duan, J. Li, P. Shao, Z. Lang, L. Bao, Y. Zhang, Z. Lin, B. Wang, *Angew. Chem. Int. Ed.* **2020**, *59*, 3905; *Angew. Chem.* **2020**, *132*, 3933; g) D. K. Nandakumar, S. K. Ravi, Y. Zhang, N. Guo, C. Zhang, S. C. Tan, *Energy Environ. Sci.* **2018**, *11*, 2179.

[5] H. Yao, P. Zhang, Y. Huang, H. Cheng, C. Li, L. Qu, *Adv. Mater.* **2019**, *31*, 1905875.

[6] a) R. Li, Y. Shi, M. Alsaedi, M. C. Wu, L. Shi, P. Wang, *Environ. Sci. Technol.* **2018**, *52*, 11367; b) A. Entezari, M. Ejeian, R. Wang, *ACS Mater. Lett.* **2020**, *2*, 471–477; c) D. K. Nandakumar, Y. Zhang, S. K. Ravi, N. Guo, C. Zhang, S. C. Tan, *Adv. Mater.* **2019**, *31*, 1806730; d) L. Yang, S. K. Ravi, D. K. Nandakumar, F. I. Alzakia, W. Lu, Y. Zhang, J. Yang, Q. Zhang, X. Zhang, S. C. Tan, *Adv. Mater.* **2019**, *31*, 1902963.

[7] A. Karmakar, P. G. M. Mileo, I. Bok, S. B. Peh, J. Zhang, H. Yuan, G. Maurin, D. Zhao, *Angew. Chem. Int. Ed.* **2020**, *59*, 11003–11009.

[8] a) J. Xu, T. Li, J. Chao, S. Wu, T. Yan, W. Li, B. Cao, R. Wang, *Angew. Chem. Int. Ed.* **2020**, *59*, 5202; *Angew. Chem.* **2020**, *132*, 5240; b) R. Y. Li, Y. Shi, M. C. Wu, S. Hong, P. Wang, *Nano Energy* **2020**, *67*, 104255; c) F. Ni, P. Xiao, N. Qiu, C. Zhang, Y. Liang, J. Gu, J. Xia, Z. Zeng, L. Wang, Q. Xue, T. Chen, *Nano Energy* **2020**, *68*, 104311.

[9] a) X. Wang, X. Li, G. Liu, J. Li, X. Hu, N. Xu, W. Zhao, B. Zhu, J. Zhu, *Angew. Chem. Int. Ed.* **2019**, *58*, 12054; *Angew. Chem.* **2019**, *131*, 12182; b) H. Qi, T. Wei, W. Zhao, B. Zhu, G. Liu, P. Wang, Z.

www.angewandte.org

© 2020 Wiley-VCH GmbH

Angew. Chem. Int. Ed. **2020**, *59*, 2–12

These are not the final page numbers!

Lin, X. Wang, X. Li, X. Zhang, J. Zhu, *Adv. Mater.* **2019**, *31*, 1903378.

[10] a) L. Brighigna, P. Montaini, F. Favilli, A. C. Trejo, *Am. J. Bot.* **1992**, *79*, 723; b) L. Brighigna, *Caryologia* **1974**, *27*, 369; c) A. Papini, G. Tani, P. Di Falco, L. Brighigna, *Flora* **2010**, *205*, 94.

[11] S. Wei, W. Lu, X. Le, C. Ma, H. Lin, B. Wu, J. Zhang, P. Theato, T. Chen, *Angew. Chem. Int. Ed.* **2019**, *58*, 16243; *Angew. Chem.* **2019**, *131*, 16389.

[12] a) F. Chen, D. Zhou, J. Wang, T. Li, X. Zhou, T. Gan, S. Handschuh-Wang, X. Zhou, *Angew. Chem. Int. Ed.* **2018**, *57*, 6568; *Angew. Chem.* **2018**, *130*, 6678; b) Y. Jian, B. Wu, X. Le, Y. Liang, Y. Zhang, D. Zhang, L. Zhang, W. Lu, J. Zhang, T. Chen, *Research* **2019**, *2019*, 2384347.

[13] F. Zhao, X. Zhou, Y. Shi, X. Qian, M. Alexander, X. Zhao, S. Mendez, R. Yang, L. Qu, G. Yu, *Nat. Nanotechnol.* **2018**, *13*, 489.

[14] a) W. Zhang, F. K. Yang, Z. Pan, J. Zhang, B. Zhao, *Macromol. Rapid Commun.* **2014**, *35*, 350; b) Y. Wang, F. Gu, L. Ni, K. Liang, K. Marcus, S. Liu, F. Yang, J. Chen, Z. S. Feng, *Nanoscale* **2017**, *9*, 18318; c) F. Ni, P. Xiao, C. Zhang, Y. Liang, J. C. Gu, L. Zhang, T. Chen, *ACS Appl. Mater. Interfaces* **2019**, *11*, 15498.

[15] J. Pan, M. Yang, L. Luo, A. Xu, B. Tang, D. Cheng, G. Cai, X. Wang, *ACS Appl. Mater. Interfaces* **2019**, *11*, 7338.

[16] a) E. T. Kang, K. G. Neoh, K. L. Tan, *Surf. Interface Anal.* **1992**, *19*, 33; b) P. Pfluger, M. Krounbi, G. B. Street, G. Weiser, *J. Chem. Phys.* **1983**, *78*, 3212.

[17] a) L. Zhou, Y. Tan, D. Ji, B. Zhu, P. Zhang, J. Xu, Q. Gan, Z. Yu, J. Zhu, *Sci. Adv.* **2016**, *2*, e1501227; b) P. Xiao, J. He, F. Ni, C. Zhang, Y. Liang, W. Zhou, J. Gu, J. Xia, S.-W. Kuo, T. Chen, *Nano Energy* **2020**, *68*, 104385.

[18] a) X. Zhou, Y. Guo, F. Zhao, G. Yu, *Acc. Chem. Res.* **2019**, *52*, 3244; b) Y. Guo, F. Zhao, X. Zhou, Z. Chen, G. Yu, *Nano. Lett.* **2019**, *19*, 2530; c) X. Hu, J. Zhu, *Adv. Funct. Mater.* **2020**, *30*, 1907234.

© 2020 Wiley-VCH GmbH

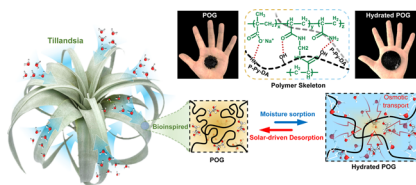**These are not the final page numbers!** ↗↗

Research Articles

Water Harvesting

F. Ni, N. Qiu, P. Xiao,* C. Zhang, Y. Jian,
Y. Liang, W. Xie, L. Yan,
T. Chen* ——————— ▄▄▄▄–▄▄▄▄

Tillandsia-Inspired Hygroscopic
Photothermal Organogels for Efficient
Atmospheric Water Harvesting

Tillandsia-inspired hygroscopic photothermal organogel (POG) is developed to realize atmospheric water harvesting. The combination of designable hydrophilic co-polymeric skeleton, hygroscopic liquid medium, and photothermic component endows POG continuous, high-efficient moisture sorption and effective solar-heating water releasing.